



Enhancing mechanical properties of friction stir welded 2219Al-T6 joints at high welding speed through water cooling and post-welding artificial ageing



Z. Zhang, B.L. Xiao, Z.Y. Ma*

Shenyang National Laboratory for Materials Science, Institute of Metal Research, Chinese Academy of Sciences, 72 Wenhua Road, Shenyang 110016, China

ARTICLE INFO

Article history:

Received 19 March 2015

Received in revised form 4 June 2015

Accepted 4 June 2015

Available online 9 June 2015

Keywords:

Aluminium alloys

Friction stir welding

Ageing

Microstructure

Mechanical properties

ABSTRACT

The effect of water cooling and post-welding artificial ageing on the microstructure and mechanical properties of 5.6-mm thick friction stir welded (FSW) 2219Al-T6 joints was subjected to detailed investigations. Sound FSW joints could be produced at the investigated welding speeds of 100–800 mm/min under both water-cooling and air-cooling conditions. The FSW thermal cycle resulted in a low hardness zone (LHZ) on both the retreating side and the advancing side. Water cooling did not exert an obvious effect on the hardness value and location of the LHZs but slightly improved the tensile strength of the FSW 2219Al-T6 joints at welding speeds of 100 and 400 mm/min. After post-welding artificial ageing, the hardness of LHZs and tensile strength of FSW 2219Al-T6 joints were substantially enhanced for all welding speeds and the strength increment increased with increases in the welding speed from 100 to 800 mm/min, attributable to increased precipitation of Al₂Cu phases in both the LHZs and the nugget zone. A combination of high welding speed and post-welding artificial ageing is proven to be the optimal path to improving the mechanical properties of FSW 2219Al-T6 joints, with a maximum joint efficiency of 91% obtained.

© 2015 Elsevier Inc. All rights reserved.

1. Introduction

Due to the good strength and fracture properties between –200 and +200 °C, 2219 aluminium alloy has been widely used in aerospace applications, especially in the fabrication of propellant storage tanks [1, 2]. 2219Al alloy is considered to possess good weldability and can be easily welded using conventional fusion welding processes. However, the joint efficiencies are as low as 50–60% [3,4]. Moreover, porosity is unavoidable in the fusion weld of 2219Al alloy due to melting and resolidification under high heat input, inhibiting the mechanical properties of the fusion weld.

Since friction stir welding (FSW) was invented by TWI in 1991 [5], high-quality FSW joints without pores or cracking have been obtainable because of the low heat input and the absence of melting and solidification processes. Currently, FSW is being applied to the aerospace, automotive, and shipbuilding industries and is attracting an increasing amount of research interest [6].

For FSW precipitation-hardened (2xxx, 6xxx, and 7xxx) aluminium alloys, it has been generally reported that the heat-affected zone (HAZ) is the low hardness zone (LHZ) due to significant dissolution/coarsening of the precipitates during the FSW thermal cycle [7–13]. For the 2219Al-

T6 alloy, although the FSW joints have been reported to have better joint efficiency compared to the fusion welded joints, the gap between the strength values of the base metal (BM) and the FSW joints is still large (>25%) due to the softening problem of the HAZ [7–9].

In previous studies, several methods have been adopted to enhance the mechanical properties of FSW 2219Al-T6 joints [8–11]. Under the air-cooling (AC) condition, Chen et al. [8] and Liu et al. [9] reported that, at a constant rotational rate of 800 rpm, the tensile strength of FSW 2219Al-T6 joints increased when the welding speed was increased from 60 to 220 mm/min, but void defects were produced at a high welding speed of 300 mm/min. It is reported that water cooling is an effective method to enhance the mechanical properties of precipitation-hardened aluminium alloys [10]. Under the water-cooling (WC) condition, Zhang et al. [11] reported that water cooling increased the tensile strength of FSW 2219Al-T6 joints from 324 to 341 MPa at a rotational rate of 800 rpm and a welding speed of 100 mm/min. Liu et al. [12] revealed that the FSW 2219Al-T6 joints obtained with water cooling at a constant rotational rate of 800 rpm and welding speeds of 50–150 mm/min fractured at either the HAZ or the nugget zone (NZ); void defects were produced when the welding speed increased from 150 to 200 mm/min. Moreover, Liu et al. [8] investigated the effect of post-weld heat treatment on the mechanical properties of FSW 2219Al-T6 joints at a rotational rate of 800 rpm and welding speeds of 60–220 mm/min and reported that post-weld artificial ageing enhanced the tensile strength of the FSW 2219Al-T6 joints.

* Corresponding author.

E-mail address: zyrna@imr.ac.cn (Z.Y. Ma).

Table 1
Chemical compositions and mechanical properties of 2219Al-T6 rolled plate.

Chemical composition								Mechanical properties		
Cu	Mg	Mn	Fe	Si	Zn	Ti	Al	YS, MPa	UTS, MPa	El, %
5.8–6.8	0.02	0.2–0.4	0.2	0.2	0.1	0.2–0.1	Bal	342	442	18

The above studies indicate that increasing the welding speed and adopting water cooling and post-weld artificial ageing are effective methods for enhancing the mechanical properties of FSW 2219Al joints, but void defects are easily formed at higher welding speeds (higher than 300 mm/min) in both AC and WC conditions [8,9,11,12]. Recently, Zhang et al. [13] reported that sound FSW 2219Al-T6 joints could be obtained at a welding speed as high as 800 mm/min with a rotational rate of 800 rpm by adjusting the plunge depth, and the tensile strength of the FSW joints was further increased at 800 mm/min.

Clearly, further increasing the tensile strength of the FSW 2219Al-T6 joints is possible by optimizing the welding parameters. Based on the aforementioned previous work, it is worthwhile to examine the possibility of further improving the mechanical properties of FSW 2219Al joints by adopting water cooling and post-weld artificial ageing at welding speeds as high as 800 mm/min.

In this study, the effect of water cooling and post-weld artificial ageing on the microstructures and mechanical properties of FSW 2219Al-T6 joints obtained at a wide range of welding speeds, from 100 to 800 mm/min, was subjected to detailed investigation. The aim of this work is to (a) explore the optimal path for improving the mechanical properties of FSW 2219Al-T6 joints and (b) elucidate the mechanism of influence of water-cooling and post-weld artificial ageing on the microstructures and mechanical properties of FSW 2219Al-T6 joints.

2. Experimental procedure

The base material used in this study was a 6.5-mm thick commercial Alclad 2219Al-T6 rolled plate. The nominal chemical compositions and tensile properties of the plate are listed in Table 1. These plates, with a length of 400 mm and a width of 90 mm, were machined on both sides to 5.6-mm thickness to remove the Alclads and then butt-welded along the rolling direction with a tool tilt angle of 2.75° using an FSW machine under two different cooling conditions: (a) normal AC without any external thermal conditioning and (b) submerged WC, by immersing the plates and welding tools into room-temperature flowing water during FSW.

Three welding parameters were selected by fixing the rotational rate at 800 rpm and increasing the welding speed from 100 to 800 mm min⁻¹, as shown in Table 2. Specifications of the welding tool included a shoulder diameter of 20 mm, a pin diameter of 8 mm, and a pin length of 5.4 mm with a standard machine screw type frustum cone-like thread. The FSW samples were subjected to either natural ageing at room temperature for more than 10 days or artificial ageing

Table 2
Welding parameters of FSW 2219Al-T6 joints.

Cooling conditions	Rotational rate (R), rpm	welding speed (V), mm/min	Sample designation
Air cooling	800	100	AC-800-100
	800	400	AC-800-200
	800	800	AC-800-800
Water cooling	800	100	WC-800-100
	800	400	WC-800-400
	800	800	WC-800-800
Air cooling + artificial ageing	800	100	AC-800-100-AA
	800	400	AC-800-400-AA
	800	800	AC-800-800-AA

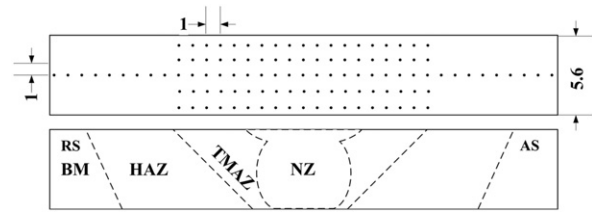


Fig. 1. Schematic illustration of FSW 2219Al-T6 joints for microhardness test, together an indication of various zones across the weld (BM, HAZ, TMAZ, and NZ).

(AA) at 160 °C for 16 h. The FSW samples were designated in abbreviated forms. For example, sample AC-800-100-AA denotes the sample welded at a rotational rate of 800 rpm and a welding speed of 100 mm min⁻¹ under a normal AC condition with 16 h of artificial ageing at 160 °C.

Vickers microhardness measurement was conducted on the cross-section of FSW 2219Al-T6 joints perpendicular to the welding direction using an automatic testing machine (LM-247AT, LECO Corporation, St. Joseph, MI, USA) under a load of 500 g for 13 s. First, the single hardness profile of the joints from the NZ to the BM was obtained along the mid-thickness of the cross-section. However, the single hardness profile cannot predict the fracture behaviour of the joints because of the limited number of data points at the lowest hardness zone. Therefore, hardness distribution maps were obtained by measuring a total of five test lines through the cross-section at an interval of 1 mm, with a total of 105 indentations. In each line, there were 21 indentations that extended from the centre to as far as 10 mm on both the retreating side (RS) and the advancing side (AS). The schematic illustration for a microhardness test, together with an indication of various zones across the joint (BM, HAZ, TMAZ, and NZ) is shown in Fig. 1.

All the samples were cross-sectioned from the joints perpendicular to the welding direction using an electrical discharge machine (DK7732, Kedi CNC Machine Tool Co., Ltd, Taizhou, China). Metallographic observation was carried out by optical microscopy (OM, Axiovert 200 MAT, Carl Zeiss Inc., Oberkochen, Germany). The samples for OM were ground, polished, and then etched using Keller's reagent (190 ml of water, 2 ml of hydrofluoric acid, 3 ml of hydrochloric acid, and 5 ml of nitric acid). The precipitate distributions in as-welded joints were observed by transmission electron microscopy (TEM, Tecnai 20, FEI Company, Hillsboro, Oregon, USA). Thin foils for TEM observation, which were cut from corresponding locations in the weld using an electrical-discharge machine, were prepared by jet electropolishing using a solution of 70% methanol and 30% nitric acid at 233 K (−30 °C) and 19 V. Much care was taken to ensure location-to-location correspondence between the observations and hardness measurements.

In order to obtain the real mechanical properties and fracture locations of the FSW joints, the joint surfaces of tensile specimens were planed with abrasive paper to ensure an equal cross-sectional area at various locations of the joints. The tensile specimens with a gauge length of 40 mm were prepared according to ASTM: E8-M11 guidelines. The configuration and size of the transverse tensile specimens are shown in Fig. 2. Room-temperature tensile tests were carried out at a strain rate of 6 × 10⁻⁴ s⁻¹ and the tensile properties of each sample reported were averages of three test results. The fracture surfaces of the failed specimens were examined by scanning electron microscopy (SEM, Quanta-600, FEI Company, Hillsboro, USA).

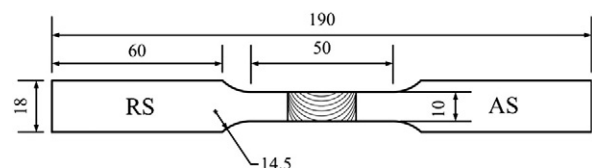


Fig. 2. Configuration and size of tensile specimen.

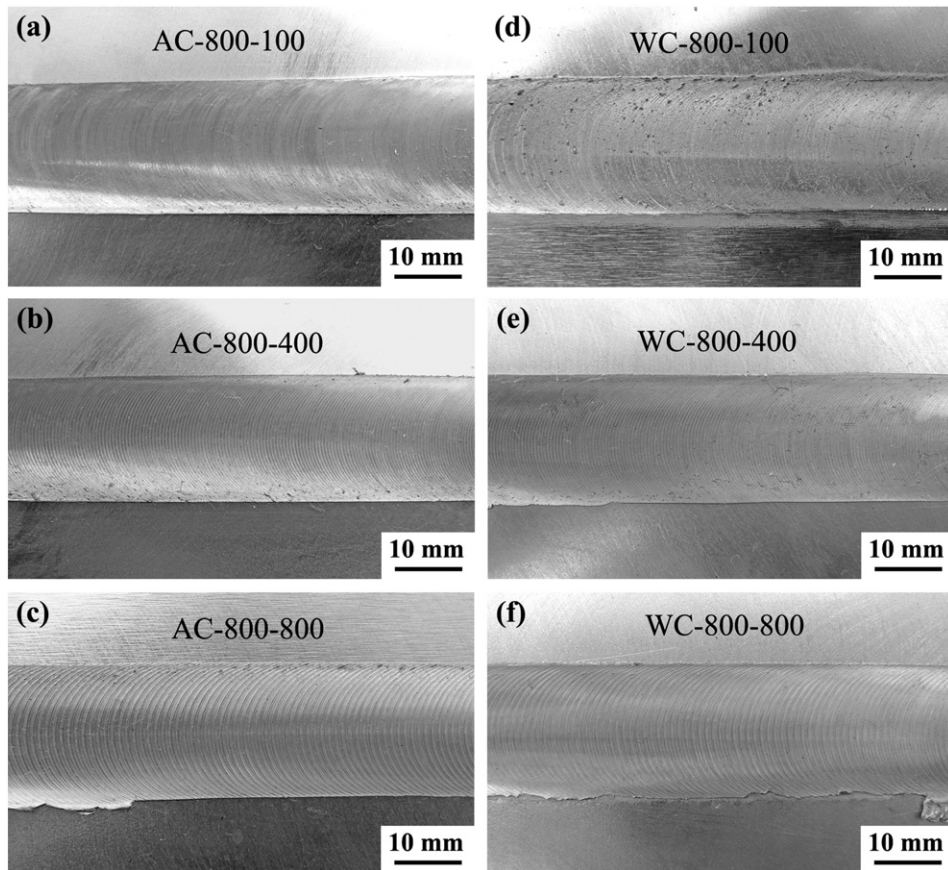


Fig. 3. Surficial morphologies of FSW 2219Al-T6 joints: (a) AC-800-100 [12], (b) AC-800-400 [12], (c) AC-800-800 [12], (d) WC-800-100, (e) WC-800-400, and (f) WC-800-800.

3. Results

3.1. Joint quality

Fig. 3 shows the macrographs of the upper surfaces of the FSW 2219Al-T6 joints under AC and WC conditions. At the welding speed of 100 mm/min, the joint surface of the AC sample (AC-800-100) was smooth (Fig. 3a), while that of the WC sample (WC-800-100) exhibited a little delamination (Fig. 3d). When the welding speed was further increased to 400 and 800 mm/min, all the FSW joint surfaces became smooth (Fig. 3b, c, e, and f).

Fig. 4 shows the cross-sectional macrostructures of the transverse cross-sections of the FSW 2219Al-T6 joints. No welding defects were detected in any of the FSW joints. Three microstructural zones, the NZ, TMAZ, and HAZ, were discernible in the FSW joint (Fig. 4a). The onion ring structure was clearly observed in the NZ of the AC-800-100 sample but was blurry in the shrunken NZ of the WC-800-100 sample (Fig. 4a and d). In the AC FSW joints, when the welding speed was increased from 100 mm/min to 400 and 800 mm/min, comparatively small NZs with indistinct onion rings were observed in samples AC-800-400 and AC-800-800 (Fig. 4b and c). However, under the WC condition, the shapes of the NZs were largely unchanged in samples WC-800-400 and WC-800-800 (Fig. 4e and f).

the thermo-mechanically affected zone (TMAZ), and the HAZ, were discernible in the FSW joint (Fig. 4a). The onion ring structure was clearly observed in the NZ of the AC-800-100 sample but was blurry in the shrunken NZ of the WC-800-100 sample (Fig. 4a and d). In the AC FSW joints, when the welding speed was increased from 100 mm/min to 400 and 800 mm/min, comparatively small NZs with indistinct onion rings were observed in samples AC-800-400 and AC-800-800 (Fig. 4b and c). However, under the WC condition, the shapes of the NZs were largely unchanged in samples WC-800-400 and WC-800-800 (Fig. 4e and f).

3.2. Microhardness map

Fig. 5 depicts the microhardness profiles of the FSW 2219Al-T6 joints under various conditions. The effect of welding speed on the hardness

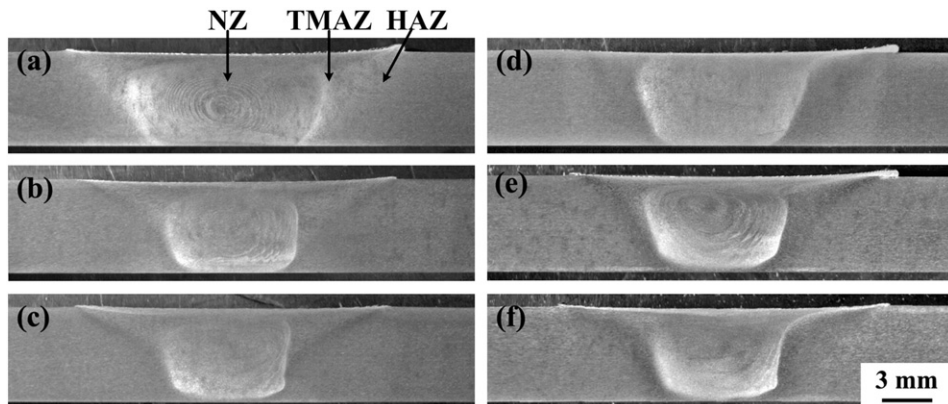


Fig. 4. Cross-sectional macrostructures of FSW 2219Al-T6 joints: (a) AC-800-100 [12], (b) AC-800-400 [12], (c) AC-800-800 [12], (d) WC-800-100, (e) WC-800-400, and (f) WC-800-800.

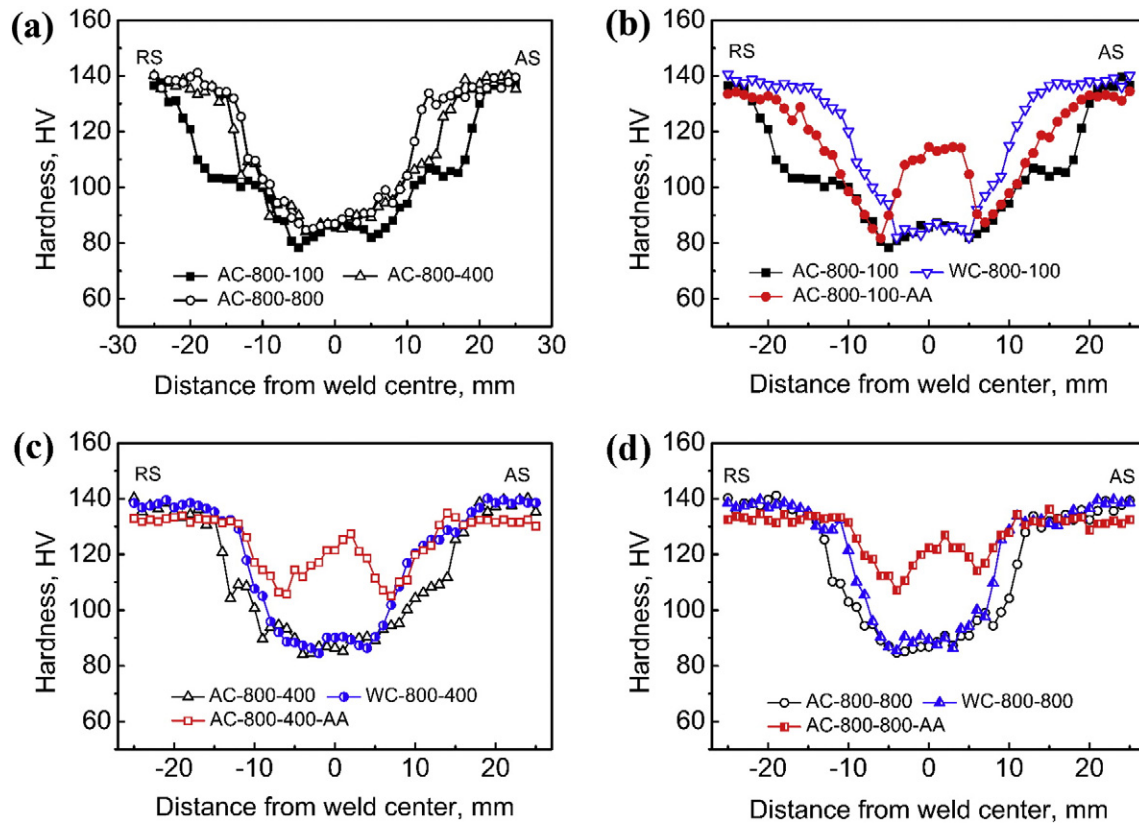


Fig. 5. Microhardness profiles of FSW 2219Al-T6 joints showing (a) effect of welding speed for a rotational rate of 800 rpm; effect of post-weld artificial ageing and water cooling at (b) 100 mm/min, (c) 400 mm/min, and (d) 800 mm/min for a rotational rate of 800 rpm.

profiles of the AC FSW joints is shown in Fig. 5a. Generally, all the hardness profiles exhibited a “W” shape with a low hardness zone (LHZ) on both the AS and the RS of the FSW joints. The hardness of the LHZ on the RS was lower than that on the AS. At a constant rotational rate of 800 rpm, increasing the welding speed from 100 to 400 mm/min caused the hardness of the LHZ to increase significantly to nearly the same value as that of the NZ. However, the variation in hardness of the FSW joints was negligible when the welding speed was further increased from 400 to 800 mm/min (Fig. 5a).

The effect of water cooling and post-weld artificial ageing on the hardness profiles of the FSW 2219Al-T6 joints at welding speeds of 100, 400, and 800 mm/min with a constant rotational rate of 800 rpm is shown in Fig. 5b–d, respectively. At the low welding speed of 100 mm/min, water cooling hardly changed the hardness of the NZ and LHZs but obviously narrowed the width of the softened region (including the NZ, TMAZ, and HAZ); post-weld artificial ageing significantly enhanced the microhardness of the NZ but only slightly improved the hardness of the LHZs (Fig. 5b). At higher welding speeds of

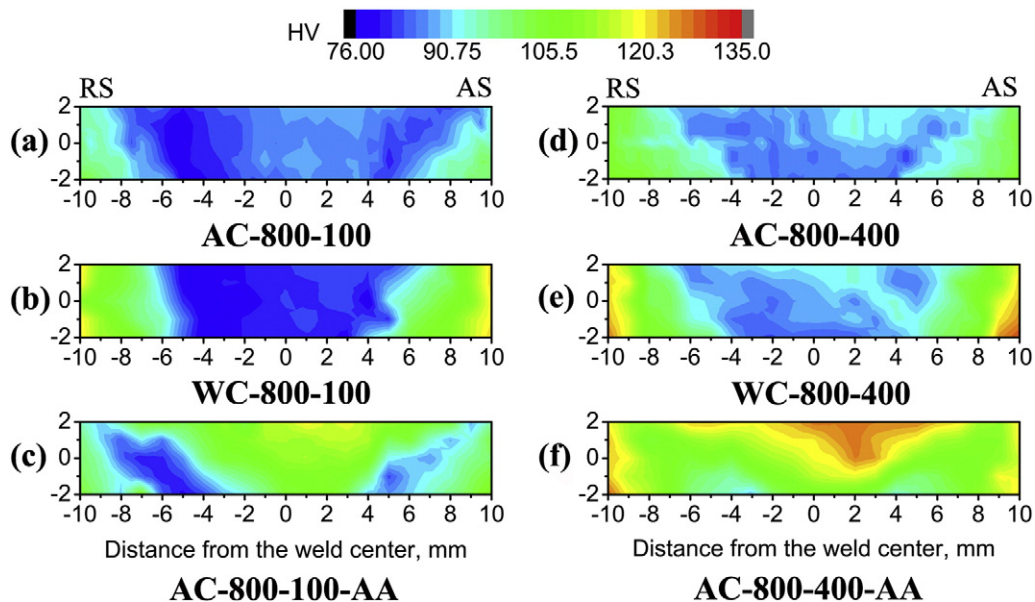


Fig. 6. Microhardness contour maps of samples (a) AC-800-100 [12], (b) WC-800-100, (c) AC-800-100-AA, (d) AC-800-400 [12], (e) WC-800-400-, and (f) AC-800-400-AA.

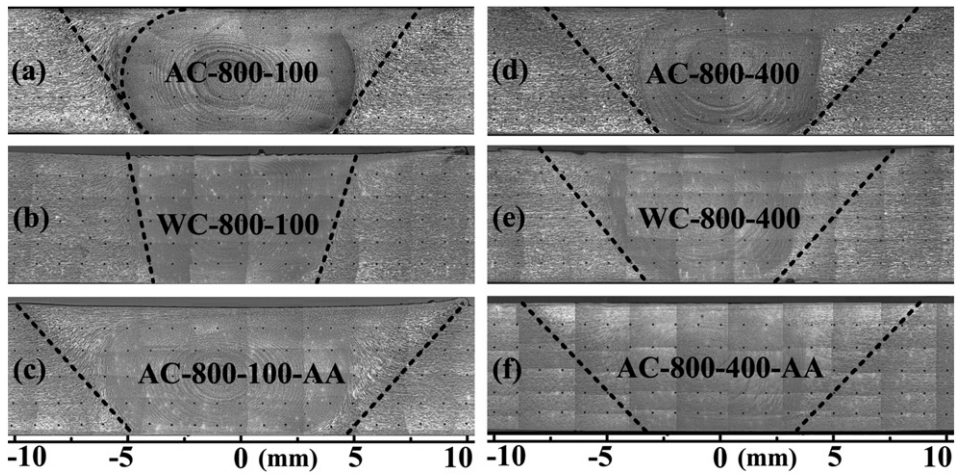


Fig. 7. Locations of LHZs (marked by the black dotted line) of samples (a) AC-800-100 [12], (b) WC-800-100, (c) AC-800-100-AA, (d) AC-800-400 [12], (e) WC-800-400, and (f) AC-800-400-AA.

400 and 800 mm/min, water cooling did not alter the hardness of the NZ and LHZs but slightly narrowed the width of the softened region; post-weld artificial ageing treatment considerably enhanced the hardness of the NZ and LHZs (Fig. 5c and d).

Figs. 6 and 7 show the microhardness contour maps and macrographs with the hardness points of samples 800–100 and 800–400 under both AC and WC conditions. At the low welding speed of 100 mm/min, two LHZs were obviously observed on both the RS and the AS under the AC

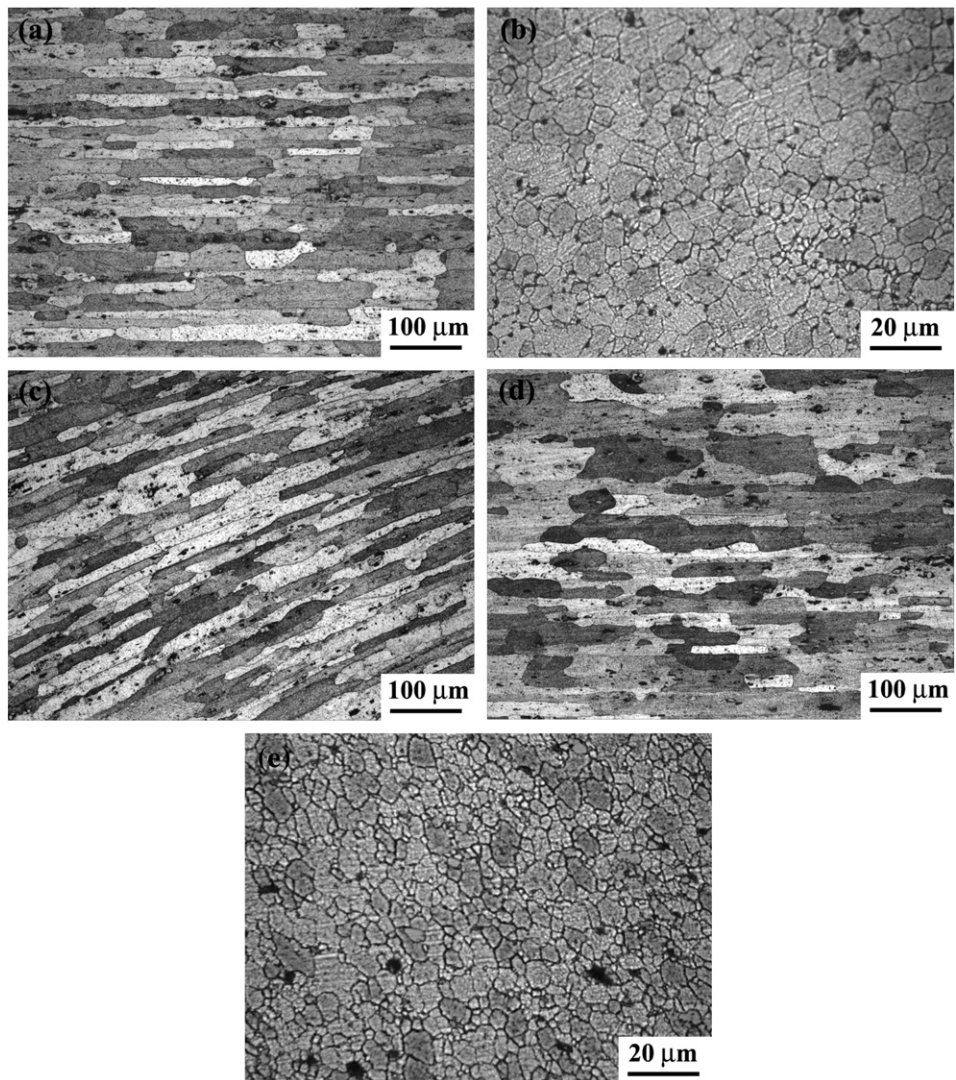


Fig. 8. OM images of (a) BM, (b) NZ, (c) TMAZ, and (d) HAZ of sample AC-800-400, (e) NZ of sample WC-800-400.

condition (Fig. 6a), with the LHZs being generally located at the NZ/TMAZ interfaces (Fig. 7a). Water cooling exerted no recognizable effect on the hardness of the LHZs but altered the distribution of the LHZs (Figs. 6b and 7b). After post-weld artificial ageing, the hardness was largely increased in the NZ and was slightly increased in the LHZs, and the LHZs were located in the HAZs (Figs. 6c and 7c).

At the middle welding speed of 400 mm/min, the LHZs were generally located at the HAZs under the AC condition (Figs. 6d and 7d), and water cooling did not change the hardness and distribution of the

LHZs (Figs. 6e and 7e). However, post-weld artificial ageing largely enhanced the hardness of both the NZ and LHZs (Figs. 6f and 7f).

3.3. Microstructure

Fig. 8a–d shows the OM micrographs of the BM, NZ, TMAZ, and HAZ of the AC-800–400 sample. It can be seen that the elongated grains of the BM resulting from the rolling process are 100–200 μm long and approximately 10–50 μm wide (Fig. 8a). At the NZ, the microstructure is

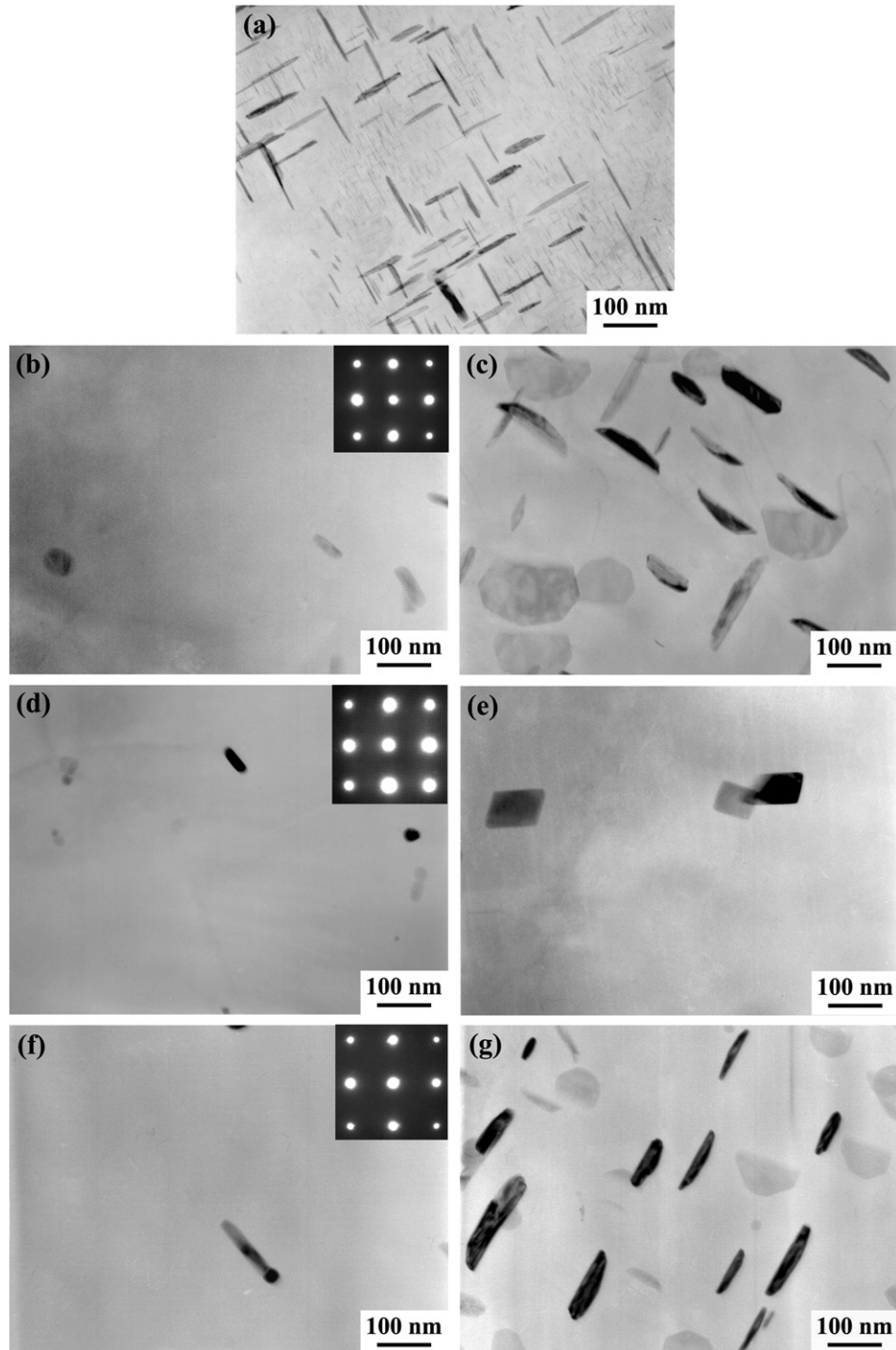


Fig. 9. Bright-field TEM micrographs and associated diffraction patterns in [100] zone axis: (a) BM; (b) NZ and (c) LHZ of the AC-800-100 sample; (d) NZ [12] and (e) LHZ of the AC-800-400 sample; and (f) NZ and (g) LHZ of the WC-800-100 sample.

characterized by the fine and equiaxed recrystallized grains (about 15 μm) arising from the severe plastic deformation and thermal exposure during welding (Fig. 8b). Upward-elongated grains were observed in the TMAZ (Fig. 8c), which underwent less plastic deformation and lower heat input. Thus there was no recrystallization in this zone. Notably coarsened grains were observed in the HAZ (Fig. 8d), in which plastic deformation was absent and only heat input played a role. Fig. 8e shows the OM micrographs of the NZ of the WC-800-400 sample. It can be seen that the grain size of its NZ (about 4 μm) is much finer compared with that of the NZ of the AC-800-400 sample (about 8 μm).

Fig. 9a–g shows the bright-field TEM images of the BM, NZ, and LHZs on the RSs of samples AC-800-100, AC-800-400, and WC-800-100, respectively. Needle-shaped Al_2Cu precipitates of different sizes are uniformly distributed; the large ones are about 80–100 μm in length and the small ones are about 10–20 μm in length (Fig. 9a). In the AC-800-100 sample, only a few Al_2Cu precipitates were observed in the NZ and the diffraction pattern showed that there were no Guinier-Preston (GP) zones in the NZ (Fig. 9b). In the LHZ, coarse Al_2Cu precipitates (about 100–150 μm in length and 30–50 μm in width) with a decreased density compared with those in the BM were observed (Fig. 9c). Compared with that of the AC-800-100 sample, the microstructure characteristic of the NZ was essentially unchanged in samples AC-800-400 and WC-800-100 (Fig. 9d and f); however the density of the coarse Al_2Cu precipitates in the LHZ was significantly decreased in the AC-800-400 sample and essentially unchanged in the WC-800-100 sample (Fig. 9e and g).

Fig. 10a–d shows the bright-field TEM images of the NZ and LHZs on the RSs of samples AC-800-100-AA and AC-800-400-AA. In the AC-800-100-AA sample, the NZ contained substantial needle-shaped Al_2Cu precipitates (Fig. 10a), which are similar to those found in the BM (Fig. 9a), and the Al_2Cu precipitates are smaller in size and lower in density in the LHZ than those in the AC-800-100 sample (Figs. 10b and 8c). In the AC-800-400-AA sample, the microstructure and characteristics of the NZ (Fig. 10c) were nearly identical to those of the AC-800-100-AA sample (Fig. 10a); however, substantial needle-shaped and coarse Al_2Cu

precipitates were observed in the LHZ (Fig. 10d) compared to that of the AC-800-100 sample (Fig. 9e).

3.4. Tensile properties and fracture behaviour

The tensile strengths of the FSW 2219Al-T6 joints under different conditions are shown in Table 3, which reveals three important findings. First, in the AC FSW joints obtained at the constant rotational rate of 800 rpm, the tensile strength increased considerably with increases in the welding speed from 100 to 400 mm/min but only slightly increased with further increases in the welding speed from 400 to 800 mm/min. Second, water cooling enhanced the tensile strength of samples AC-800-100 and AC-800-400 slightly, but hardly improved the tensile strength of the AC-800-800 sample. Third, post-weld artificial ageing enhanced the tensile strength of the FSW 2219Al-T6 joints significantly, and more importantly, the strength increment increased with increases in the welding speed. This means that post-weld artificial ageing produces larger enhancement effects on the strength of the joints at higher welding speeds.

In order to accurately locate the tensile fracture location of the FSW joints, the cross-sections of the failed specimens were etched. Under the investigated parameters, all the FSW joints fractured along the LHZs on the RS. The typical fracture locations of samples AC-800-100, WC-800-100, and AC-800-100-AA are shown in Fig. 11. It can be seen that samples AC-800-100 and WC-800-100 fractured along the NZ/TMAZ interface on the RS (Fig. 11a and b). After post-weld artificial ageing, the AC-800-100-AA sample fractured at the HAZ on the RS, with the shear fracture path at a $\sim 45^\circ$ angle to the tensile axis (Fig. 11c). It should be noted that samples AC-800-400, AC-800-800, WC-800-400, WC-800-800, AC-800-400-AA, and AC-800-800-AA fractured along the LHZ on the RS.

Figs. 12 and 13 show the typical SEM fractographs of samples AC-800-100, WC-800-100, and AC-800-100-AA. The macroscopic images showed the embossed fracture surface for the AC-800-100 sample, the mixed fracture surface with two distinct patterns for the WC-800-100 sample and the flat fracture surface for the AC-800-100-AA sample (Fig. 12a–c). The magnified images of positions A, B and D showed the

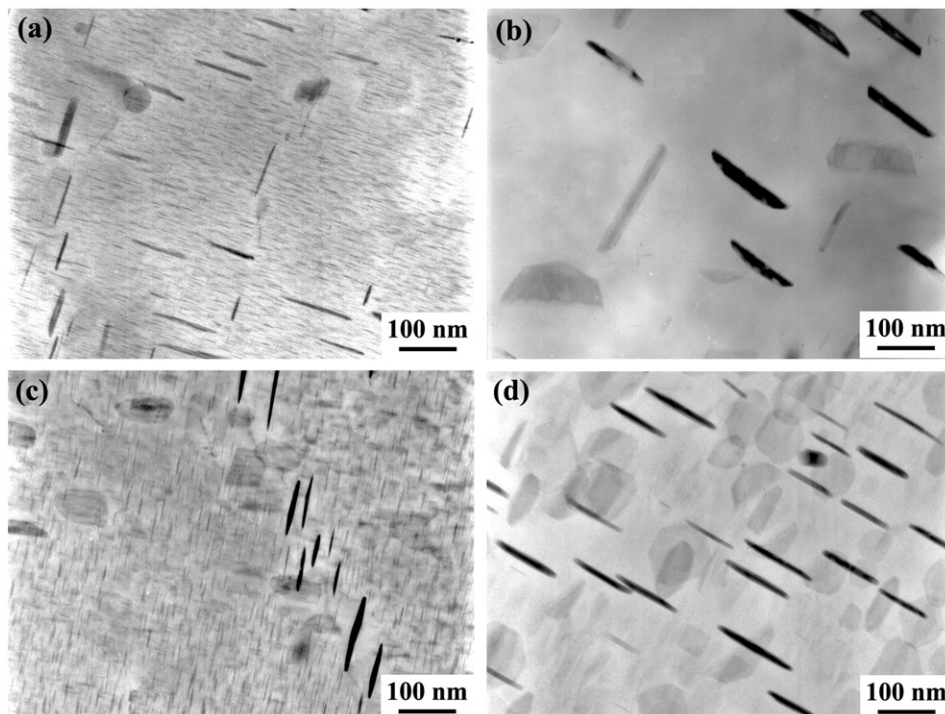


Fig. 10. Bright-field TEM micrographs: (a) NZ and (b) LHZ of the AC-800-100-AA sample; and (c) NZ and (d) LHZ of the AC-800-400-AA sample.

Table 3
Transverse tensile properties of FSW 2219Al-T6 joints.

Sample designation	UTS, MPa	UTS _{FSW} /UTS _{BM} , %
AC-800-100	320 ± 3	72
AC-800-400	341 ± 1	77
AC-800-800	349 ± 2	79
WC-800-100	332 ± 2	72
WC-800-400	352 ± 1	80
WC-800-800	352 ± 2	80
AC-800-100-AA	339 ± 2	76
AC-800-400-AA	386 ± 2	87
AC-800-800-AA	403 ± 1	91

similar characteristic of ductile rupture (Fig. 13a, b and d). However, the magnified image of position C in the WC-800-100 sample exhibited the cleavage fracture (Fig. 13c).

4. Discussion

4.1. Relationship between water cooling and joint quality

Under the AC condition, Zhang et al. [13] reported that sound FSW 2219Al-T6 joints could be obtained at lower rotational rates of 400–800 rpm and welding speeds of 100–800 mm/min, while higher rotational rates of 1200–1600 rpm easily led to tunnel and void defects. Under the WC condition, the investigated welding parameters and joint quality of the FSW 2219Al-T6 joints in the previous studies [12,14] and this study are summarized in Table 4. In the previous studies [12,14], the void defects were generally produced at higher rotational rates (≥ 1400 rpm) or high welding speeds (≥ 200 mm/min) in the WC FSW joints. However, this study indicated that a defect-free WC FSW joint could be produced at a wide range of welding speeds from 100 to 800 mm/min, which is not in complete agreement with the previous results. This difference can be explained as follows.

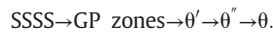
According to the relationship between the material flow characteristic and joint quality during FSW, three material flow states, insufficient material flow, balanced material flow, and excessive material flow states are identified [15,16]. The balanced material flow state is an ideal welding state without the occurrence of welding defects, which is achieved by a reasonable combination of rotational rate, welding speed, and plunge depth. However, the defects were easily produced in the insufficient and excess material flow states, which generally resulted from high welding speed and high rotational rate, respectively [16].

Besides the rotational rate and welding speed, the plunge depth was also an important welding parameter for FSW. The low welding speed of 100 mm/min led to a long stirring time and adequate material flow for the rotational rate of 800 rpm, producing a balanced material flow state. A sound FSW joint was therefore produced (Figs. 3a and 4a). Increasing the welding speed from 100 to 400 and 800 mm/min would change the material flow state from balanced to insufficient due to inadequate material flow [16]. However, this trend could be avoided by properly increasing the plunge depth of the, as shown in this study. The sound WC FSW 2219Al-T6 joints were therefore achieved at higher welding

speeds of 400 and 800 mm/min (Figs. 3e, f, 4e, and f). The void defects in the FSW 2219Al-T6 joints at high welding speeds (200 mm/min) reported in Refs. [12] and [14] may be associated with insufficient plunge depth.

4.2. Effect of post-weld artificial ageing and water-cooling on the microstructure and mechanical properties

The 2219Al alloy is a binary Al–Cu alloy and has a smooth natural ageing tendency. Its precipitation sequence from the supersaturated solid solution (SSSS) is [17]:



The original θ (Al₂Cu) precipitates in the BM are formed during artificial ageing at the temperature of 190 °C. It would coarsen at 300–400 °C and dissolve above 505 °C. During FSW, the varied positions of the FSW joints experienced different thermal cycles. The θ precipitates therefore evolved in different ways at the varied positions.

The fracture behaviour and mechanical properties of the FSW 2219Al-T6 joints were mainly dependent on the microhardness value and distribution of the LHZs, which were closely related to the precipitate distribution of the FSW joints. It has been generally reported that the LHZ is located at the HAZ in FSW precipitation-hardened aluminium alloys [7–9,11–13]. However, recently Zhang et al. [14] reported that the LHZ of the FSW 2219Al-T6 joints may be located at the NZ/TMAZ interface or the HAZ at varied welding parameters. Thus, all the microstructure evolutions of the NZ, TMAZ, and HAZ of the FSW 2219Al-T6 joints should be considered in this study.

4.2.1. Microstructure evolution of NZ

Under the AC condition, the NZ experienced severe plastic deformation and high heat input with a peak temperature of about 400–550 °C during FSW [18,19]. This resulted in the dissolution of most of the Al₂Cu precipitates as well as the coarsening of the remaining Al₂Cu precipitates (Fig. 9b and d). During post-weld artificial ageing, substantial Al₂Cu precipitates formed in the NZ of the FSW 2219Al-T6 joints (Fig. 10a and c). The hardness of the NZ of the artificially aged FSW joints therefore increased greatly (Fig. 5b–d).

Compared with the AC condition, water cooling resulted in decreased heat input in the NZ during FSW. However, the heat input during WC FSW was still enough to dissolve the Al₂Cu phases. Thus, the grains became finer, but the precipitates were essentially unchanged in the NZ in the WC joints compared with those in the AC FSW joints (Figs. 8b, e, 9b, and f). However, during the subsequent post-weld natural ageing of the FSW joints, the GP zones in the NZ did not form in all the joints (Fig. 9b, d, and f). A possible reason is that the heating and cooling processes of FSW eliminated the vacancies, which strongly slowed down the GP zone formation at room temperature after welding. Coupled with the smooth natural ageing tendency of the 2219Al alloy, the hardness of the NZ was therefore about 85–90 HV.

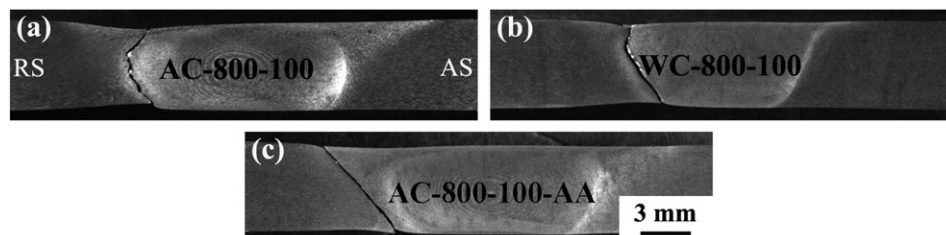


Fig. 11. Fracture locations: (a) AC-800-100 [12], (b) WC-800-100, and (c) AC-800-100-AA.

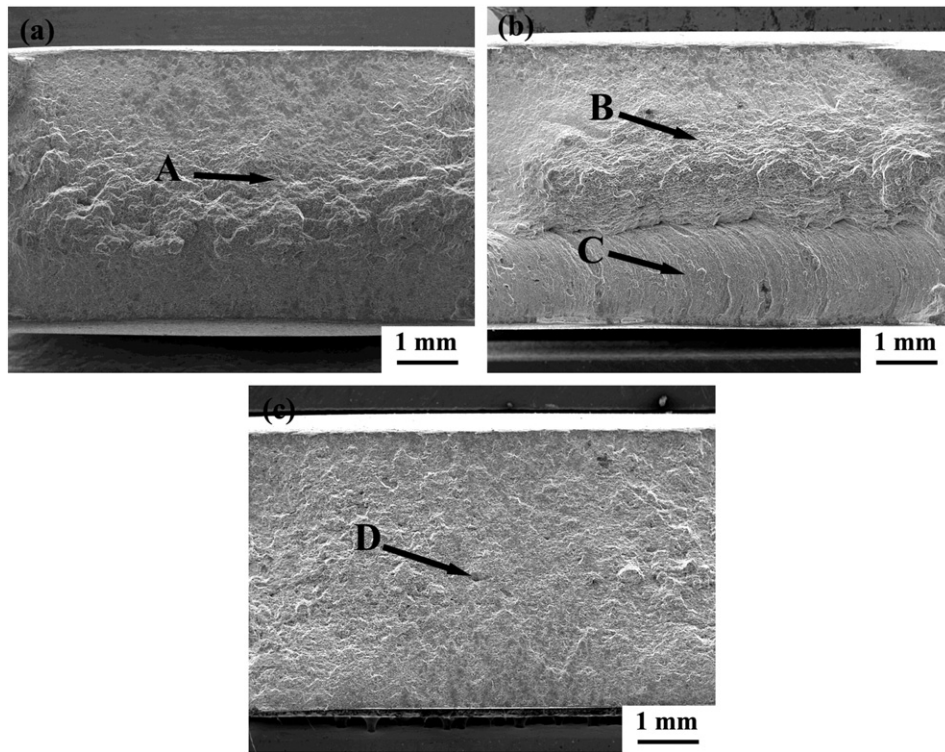


Fig. 12. Fractographs of (a) AC-800-100, (b) WC-800-100, and (c) AC-800-100-AA.

4.2.2. Microstructure evolution of LHZ and its effect on mechanical properties

During FSW of precipitation-hardened aluminium alloys, the TMAZ and HAZ experienced the thermal cycles with peak temperatures between 300 and 410 °C [20], resulting in overageing. Based on temperature measurements and microstructural examinations of the LHZs of

FSW 6061Al-T6 joints, Liu and Ma [21] proposed an isothermal-dissolution-layer (ITDL) model, which predicts that all the LHZs experienced the thermal cycles with the same peak temperature of 360–370 °C. The ITDL model was verified by numerical simulation and also proven to be applicable to the FSW joints of other precipitation-hardened aluminium alloys [22,23].

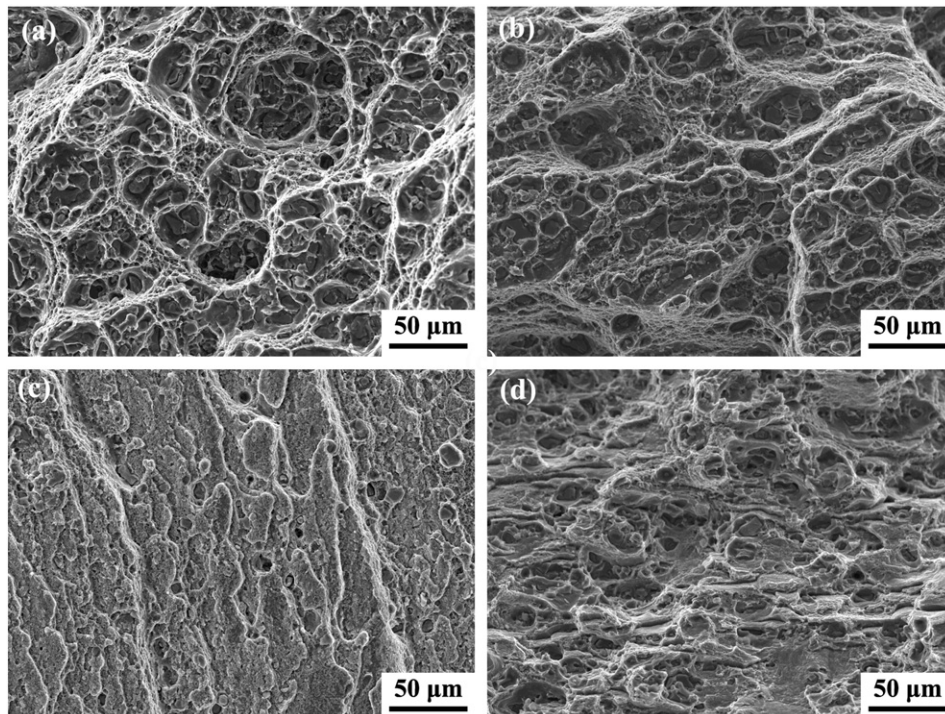


Fig. 13. Magnified micrographs of Fig. 12 from position A to position D: (a) position A, (b) position B, (c) position C, and (d) position D.

Table 4
Summary of welding parameters and joint quality of FSW 2219Al-T6 joints.

Cooling condition	Investigated welding parameters		Defective sample	Refs.
	Rotational rate	Welding speed		
Water cooling	800	100–800	None	This study
	800	50–200	800–200	[12]
	600–1400	100	1400–100	[14]

The peak temperatures of thermal cycles in the LHZs were about 400 °C for the FSW 2219Al-T6 joints [11]. The dissolution of the Al₂Cu precipitates as well as the coarsening of the remaining Al₂Cu precipitates occurred in the LHZs. In this case, there are two strengthening origins in the LHZs: the Al₂Cu phase and the solute atoms. During the post-weld artificial ageing, the solute atoms evolved into the Al₂Cu precipitates. The degree of coarsening of Al₂Cu precipitates was dependent on the duration of overageing, that is, the time above the ageing temperature of 190 °C, which was related to the welding speed and was independent of the rotational rate [21,24].

At the low welding speed of 100 mm/min, the LHZs of the AC joint experienced a long overageing duration during FSW, leading to the coarsening of most of the Al₂Cu precipitates as well as the dissolution of the few remaining Al₂Cu precipitates. After post-weld artificial ageing, only few Al₂Cu precipitates reformed in the TMAZ and HAZ of the AC-800-100-AA sample. Thus, the hardness of the NZ, TMAZ, and HAZ recovered to different degrees and the LHZ moved outwards from the NZ/TMAZ interface for the AC-800-100 sample to the HAZ for the AC-800-100-AA sample (present Figs. 5b, 6c, and 7c). Samples AC-800-100 and AC-800-100-AA fractured along their LHZs with similar rupture characteristics (Figs. 11a, c, 12a, c, 13a and d).

The Al₂Cu precipitates in the LHZs of the AC-800-100-AA sample were lower in density than those of sample AC-800-100 (Figs. 9c and 10b). Thus, the hardness in the LHZs was increased and the tensile strength of the joint was enhanced by 5.9% for the AC-800-100-AA sample (Fig. 5b and Table 5). The effect of post-weld artificial ageing was measured by the strength increment, which is defined as $(UTS_{AC+AA} - UTS_{AC}) / UTS_{AC}$ in Table 5.

Increasing the welding speed from 100 to 400 mm/min resulted in the dissolution of more Al₂Cu precipitates and the coarsening of the few remaining Al₂Cu precipitates in the LHZs of the AC FSW joint (Fig. 9e), indicating that the LHZs of the AC-800-400 sample contained many more solute atoms than those of the AC-800-100 sample. Therefore, substantial Al₂Cu precipitates formed in the LHZs of the AC-800-400-AA sample (Fig. 10d). Thus, post-weld artificial ageing considerably enhanced the hardness of LHZ, and therefore the tensile strength of the AC-800-400-AA sample was increased by 13.2% (Fig. 5c and Table 5).

The LHZs of the AC-800-800 sample experienced a shorter duration of overageing than those of the AC-800-400 sample. In this case, the LHZs of the AC-800-800 sample possessed more solute atoms than those of the AC-800-400 sample. Thus, post-weld artificial ageing resulted in a higher strength increment of 15.5% in the AC-800-800-AA sample (Table 5).

The effect of water cooling on the tensile properties of the FSW 2219Al-T6 joints in Ref. [11] and this study, measured by the strength increment, $(UTS_{WC} - UTS_{AC}) / UTS_{AC}$, are summarized in Table 6. The water cooling slightly improved the tensile strength of the FSW

2219Al-T6 joints at welding speeds of 100 and 400 mm/min but hardly enhanced the tensile strength of the joint at the high welding speed of 800 mm/min. This is due to the fact that in the AC-800-100 sample, the microhardness of the LHZs was slightly lower than that of the NZ, and the LHZs experienced a long duration of overageing. In this case, water cooling alleviated the overageing in the LHZs of the WC-800-100 sample. Therefore, water cooling altered the distribution of LHZs and improved the tensile strength of the WC-800-100 sample by 3.8% (Fig. 5b and Table 6). The altered distribution of the LHZs caused the WC-800-100 sample to fracture partially along the onion-ring in a mixed mode (Figs. 11b, 12b, 13b and c).

On increasing the welding speed from 100 to 400 mm/min, the hardness of the LHZs became nearly identical to that of the NZ, and the LHZs experienced a shorter duration of overageing in the AC-800-400 sample. Water cooling exerted a small effect on the overageing of LHZs and thereby improved the tensile strength of the WC-800-400 sample by 3.2% (Figs. 5c and 6e and Table 6). It should be noted that water cooling did not induce conspicuous changes in the hardness of the LHZs, although it slightly improved the tensile strength of the WC-800-400 sample.

By further increasing the welding speed from 400 to 800 mm/min, the duration of overageing of the WC FSW joint was further shortened. Water cooling hardly affected the overageing of the LHZs and therefore did not change the hardness of LHZs; it enhanced the tensile strength of the WC-800-800 sample by only 0.9% (Fig. 5d and Table 6).

The results of this study demonstrate the close relationship between the welding parameters, water cooling, post-weld artificial ageing, and the mechanical properties of the FSW 2219Al-T6 joints. Firstly, there are a wide range of welding speeds between 100 and 800 mm/min available for producing defect-free joints in both AC and WC conditions. Secondly, water cooling slightly improved the tensile strength of the FSW joints at welding speeds of 100 and 400 mm/min but did not enhance the tensile strength of joints at 800 mm/min. Thirdly, post-weld artificial ageing considerably enhanced the tensile strength of the FSW 2219Al-T6 joints at welding speeds of 100–800 mm/min and the strength increment increased with increases in the welding speed. Lastly, a high welding speed combined with post-weld artificial ageing is the optimal path for improving the mechanical properties of FSW 2219Al-T6 joints.

5. Conclusions

- (1) Sound FSW 2219Al-T6 joints could be obtained at welding speeds of 100–800 mm/min with a constant rotational rate of 800 rpm under both air- and water-cooling conditions.
- (2) The FSW thermal cycle resulted in the appearance of the LHZs on both the RS and the AS due to the dissolution and coarsening of

Table 5
Effect of post-weld artificial ageing on the tensile properties of FSW 2219Al-T6 joints.

Plate thickness, mm	Tensile strength				Fracture location	Refs.
	Sample	UTS _{AC} , MPa	UTS _{AC-AA} , MPa	UTS _{AC-AA} - UTS _{AC} / UTS _{AC} , %		
5.6	800–100	320	339	5.9	NZ/TMAZ interface, or HAZ on RS	This study
	800–400	341	386	13.2		
	800–800	349	403	15.5		
5.0	800–220	336	372	10.7	NZ, NZ/TMAZ interface, or HAZ on RS	[8]

Table 6

Effect of water cooling on the tensile properties of FSW 2219Al-T6 joints.

Plate thickness, mm	Tensile strength				Fracture location	Refs.
	Sample	UTS _{AC} , MPa	UTS _{WC} , MPa	UTS _{WC} – UTS _{AC} / UTS _{AC} , %		
5.6	800–100	320	332	3.8	NZ/TMAZ interface, or HAZ on RS	This study
	800–400	341	352	3.2		
	800–800	349	352	0.9		
7.5	800–100	324	341	5	NZ, NZ/TMAZ interface, or HAZ on AS	[11]

Al₂Cu precipitates. The hardness of the LHZs increased as the welding speed increased from 100 to 400 and 800 mm/min. Water cooling did not exert obvious effects on the hardness of the LHZs of FSW 2219Al-T6 joints. Post-weld artificial ageing considerably enhanced the hardness of the LHZs and moved the location of LHZs towards the weld centre.

- (3) Under the air-cooling condition, the LHZs of the FSW 2219Al-T6 joints were located at either the NZ/TMAZ interface or in the HAZ at different welding speeds. Water cooling did not change the location of the LHZs at welding speeds of 100–800 mm/min. Post-weld artificial ageing moved the LHZs from the NZ/TMAZ interface to the HAZ at the welding speed of 100 mm/min.
- (4) Water cooling slightly improved the tensile strength of the FSW 2219Al-T6 joints at welding speeds of 100 and 400 mm/min but did not enhance the tensile strength of joints at 800 mm/min. Post-weld artificial ageing considerably enhanced the tensile strength of the FSW 2219Al-T6 joints at welding speeds of 100–800 mm/min, and the strength increment increased with increases in the welding speed.
- (5) The FSW 2219Al-T6 joints fractured along the LHZs under different conditions. A high welding speed combined with post-weld artificial ageing is the optimal path for improving the mechanical properties of FSW 2219Al-T6 joints. The maximum joint efficiency (UTS_{FSW}/UTS_{BM}) of the FSW 2219Al-T6 joints was 91%.

Acknowledgements

This work was supported by the National Natural Science Foundation of China under grant no. 51331008.

References

- [1] S.R.K. Rao, G.M. Reddy, K.S. Rao, M. Kamaraj, K.P. Rao, Grain refinement through arc manipulation techniques in Al–Cu alloy GTA welds, *Mater. Sci. Eng. A* 404 (2005) 227–234.
- [2] W.F. Xu, J.H. Liu, G.H. Luan, C.L. Dong, Temperature evolution, microstructure and mechanical properties of friction stir welded thick 2219-O aluminum alloy joints, *Mater. Des.* 30 (2009) 1886–1893.
- [3] S.R.K. Rao, G.M. Reddy, K.S. Rao, M. Kamaraj, K.P. Rao, Reasons for superior mechanical and corrosion properties of 2219 aluminum alloy electron beam welds, *Mater. Charact.* 55 (2005) 345–354.
- [4] S. Malarvizh, K. Raghukandan, N. Viswanathan, Effect of post weld aging treatment on tensile properties of electron beam welded AA2219 aluminum alloy, *Int. J. Adv. Manuf. Technol.* 37 (2008) 294–301.
- [5] W.M. Thomas, E.D. Nicholas, J.C. Needham, M.G. Murch, P. Templesmith, C.J. Dawes, G.B. Patent Application No. 9125978.8, Dec 1991.
- [6] R.S. Mishra, Z.Y. Ma, Friction stir welding and processing, *Mater. Sci. Eng. R* 50 (2005) 1–78.
- [7] Y.C. Chen, H.J. Liu, J.C. Feng, Friction stir welding characteristics of different heat-treated-state 2219 aluminum alloy plates, *Mater. Sci. Eng. A* 420 (2006) 21–25.
- [8] H.J. Liu, Y.C. Chen, J.C. Feng, Effect of heat treatment on tensile properties of friction stir welded joints of 2219-T6 aluminum alloy, *Mater. Sci. Technol.* 22 (2006) 237–241.
- [9] W.F. Xu, H.J. Liu, G.H. Luan, C.L. Dong, Microstructure and mechanical properties of friction stir welded joints in 2219-T6 aluminum alloy, *Mater. Des.* 30 (2009) 3460–3467.
- [10] C. Sharma, D.K. Dwivedi, P. Kumar, Influence of in-process cooling on tensile on tensile behaviour of friction stir welded joints of AA7039, *Mater. Sci. Eng. A* 556 (2012) 479–487.
- [11] H.J. Zhang, H.J. Liu, L. Yu, Effect of water cooling on the performances of friction stir welding heat-affected zone, *J. Mater. Eng. Perform.* 21 (2012) 1182–1187.
- [12] H.J. Liu, H.J. Zhang, L. Yu, Effect of welding speed on microstructures and mechanical properties of underwater friction stir welded 2219 aluminum alloy, *Mater. Des.* 32 (2011) 1548–1553.
- [13] Z. Zhang, B.L. Xiao, Z.Y. Ma, Effect of welding parameters on microstructure and mechanical properties of friction stir welded 2219Al-T6 joints, *J. Mater. Sci.* 47 (2012) 4075–4086.
- [14] H.J. Zhang, H.J. Liu, L. Yu, Microstructure and mechanical properties as a function of rotational speed in underwater friction stir welded aluminum alloy joints, *Mater. Des.* 32 (2011) 4402–4407.
- [15] W.J. Arbegast, A flow-partitioned deformation zone model for defect formation during friction stir welding, *Scr. Mater.* 58 (2008) 372–376.
- [16] Z. Zhang, B.L. Xiao, D. Wang, Z.Y. Ma, Effect of clad layer on material flow and defect formation in friction stir welded 2024 aluminum alloy, *Metall. Mater. Trans. A* 42 (2011) 1717–1726.
- [17] G.W. Lorimer, *Precipitation Processes in Solids*, TMS-AIME, Warrendale, PA, 1978. 87.
- [18] P.A. Colegrove, H.R. Shercliff, Experimental and numerical analysis of aluminium alloy 7075-T7351 friction stir welds, *Sci. Technol. Weld. Join.* 8 (2003) 360–368.
- [19] Y.S. Sato, M. Urata, H. Kokawa, Parameters controlling microstructure and hardness during friction stir welding of precipitation-hardenable aluminum alloy 6063, *Metall. Mater. Trans. A* 33 (2002) 625–635.
- [20] W.B. Lee, Y.M. Yeon, S.B. Jung, Mechanical properties related to microstructural variation of 6061 Al alloy joints by friction stir welding, *Mater. Trans.* 45 (2004) 1700–1705.
- [21] F.C. Liu, Z.Y. Ma, Influence of tool dimension and welding parameters on microstructure and mechanical properties of friction stir welded 6061-T651 aluminum alloy, *Metall. Mater. Trans. A* 39 (2008) 2378–2388.
- [22] X.X. Zhang, B.L. Xiao, Z.Y. Ma, A transient thermal model for friction stir weld. Part I: The model, *Metall. Mater. Trans. A* 42 (2011) 3218–3228.
- [23] X.X. Zhang, B.L. Xiao, Z.Y. Ma, A transient thermal model for friction stir weld. Part II: Effects of weld conditions, *Metall. Mater. Trans. A* 42 (2011) 3229–3239.
- [24] Z. Zhang, B.L. Xiao, Z.Y. Ma, Hardness recovery mechanism in the heat-affected zone during long-term natural aging and its influence on the mechanical properties and fracture behaviour of friction stir welded 2024Al-T351 joints, *Acta Mater.* 73 (2014) 227–239.